

DISCOVERY OF A TRANSIENT GAMMA-RAY COUNTERPART TO FRB 131104

J. J. DELAUNAY^{1,3,5}, D. B. FOX^{2,3,4}, K. MURASE^{1,2,3,4}, P. MÉSZÁROS^{1,2,3,4}, A. KEIVANI^{1,3}, C. MESSICK^{1,3},
M. A. MOSTAFÁ^{1,3}, F. OIKONOMOU^{1,3}, G. TEŠIĆ^{1,3}, AND C. F. TURLEY^{1,3}

¹Department of Physics, Pennsylvania State University, University Park, PA 16802, USA

²Department of Astronomy & Astrophysics, Pennsylvania State University, University Park, PA 16802, USA

³Center for Particle & Gravitational Astrophysics, Institute for Gravitation and the Cosmos, Pennsylvania State University, University Park, PA 16802, USA

⁴Center for Theoretical & Observational Cosmology, Institute for Gravitation and the Cosmos, Pennsylvania State University, University Park, PA 16802, USA

⁵jjd330@psu.edu

ABSTRACT

We report our discovery in Swift satellite data of a transient gamma-ray counterpart (3.2σ confidence) to the fast radio burst FRB 131104, the first such counterpart to any FRB. The transient has duration $T_{90} \gtrsim 100$ s and fluence $S_\gamma \approx 4 \times 10^{-6}$ erg cm⁻², increasing the energy budget for this event by more than a billion times; at the nominal $z \approx 0.55$ redshift implied by its dispersion measure, the burst’s gamma-ray energy output is $E_\gamma \approx 5 \times 10^{51}$ erg. The observed radio to gamma-ray fluence ratio for FRB 131104 is consistent with a lower limit we derive from Swift observations of another FRB, which is not detected in gamma-rays, and with an upper limit previously derived for the brightest gamma-ray flare from SGR 1806–20, which was not detected in the radio. X-ray, ultraviolet, and optical observations beginning two days after the FRB do not reveal any associated afterglow, supernova, or transient; Swift observations exclude association with the brightest 65% of Swift gamma-ray burst X-ray afterglows, while leaving the possibility of an associated supernova at much more than 10% the FRB’s nominal distance, $D \gtrsim 320$ Mpc, largely unconstrained. Transient high-luminosity gamma-ray emission arises most naturally in a relativistic outflow or shock breakout, as for example from magnetar flares, gamma-ray bursts, relativistic supernovae, and some types of galactic nuclear activity. Our discovery thus bolsters the case for an extragalactic origin for some FRBs and suggests that future rapid-response observations might identify long-lived counterparts, resolving the nature of these mysterious phenomena and realizing their promise as probes of cosmology and fundamental physics.

Keywords: gamma-ray burst: general — gamma-ray burst: individual (FRB 131104) — intergalactic medium — radio continuum: general

1. INTRODUCTION

Fast radio bursts (FRBs) are millisecond-long bursts of coherent GHz-frequency emission (Lorimer et al. 2007; Thornton et al. 2013), now regularly discovered by radio pulsar surveys and survey facilities. Interest in this population has been stimulated by their large dispersion measures, $DM \gtrsim 300$ pc cm⁻³, which suggest an origin at cosmological distances $D \gtrsim 1$ Gpc (potentially in combination with substantial plasma densities local to the source), and by their high all-sky rate, estimated at $\mathcal{R} \approx 2100$ day⁻¹ for fluences $S_{\text{GHz}} > 2$ Jy ms (Champion et al. 2016). Using dispersion measures to infer distances in a standard cosmology (e.g., Callister et al. 2016) gives a $z \approx 0.85$ horizon for FRB detection with current facilities, yielding a lower bound

on their volumetric rate of 6700 Gpc⁻³ yr⁻¹ or 7% the rate of core collapse supernovae (Taylor et al. 2014).

FRBs are thus a dramatic feature of the radio sky and an important component of the transient activity of the local extragalactic or cosmological universe. Yet despite intensifying efforts at real-time discovery and follow-up (Petroff et al. 2015a; Ravi et al. 2015; Keane et al. 2016), along with identification (Spitler et al. 2016) and detailed studies (Scholz et al. 2016) of a single repeating source (FRB 121102), no non-radio counterpart or high-confidence host galaxy for any FRB has been found, leaving their distances, energy scales, and physical nature(s) unresolved.

In the absence of such counterparts, clues to the nature of the FRBs have accumulated primarily via ra-

dio observations. Although only FRB 121102 is currently known to repeat, most of the fainter bursts from this source would not have been detected at facilities other than Arecibo. Further FRB repeaters may wait to be discovered (e.g. FRBs 110220 and 140514; Maoz et al. 2015), though limits from less sensitive facilities (Petroff et al. 2015b) suggest they are likely a minority.

The 44% linear polarization of FRB 110523 enabled simultaneous measurement of its dispersion and rotation measures, demonstrating the presence of excess magnetized plasma along the line of sight, likely located near the source in its external host galaxy (Masui et al. 2015). This has provided substantial support for cosmological scenarios (the DM-based redshift estimate for FRB 110523 is $z \approx 0.5$), especially models with relatively young progenitors that would be associated with nuclear or star-forming regions or a surrounding supernova remnant (Masui et al. 2015; Murase et al. 2016).

One of five FRBs reported by Champion et al. (2016) exhibited a double-peaked profile, with two peaks separated by $\Delta t \approx 5$ ms (FRB 121002). This may disfavor catastrophic scenarios, e.g. binary neutron star (BNS) mergers (Champion et al. 2016).

Rapid-response observations of FRB 150418 (Keane et al. 2016) across multiple bandpasses identified a variable radio source, superposed on a $z = 0.49$ host galaxy, that was proposed as the fading afterglow of a short-hard (BNS merger) gamma-ray burst. However, subsequent observations revealed that the radio variable was in fact the galaxy’s active nucleus (AGN) rather than an afterglow (Williams & Berger 2016), leaving this FRB also without a high-confidence non-radio counterpart or host galaxy.

An FRB model invoking maser-like flaring of Galactic flare stars has also been put forward (Loeb et al. 2014). Challenges for this model include precisely reproducing the observed dispersion relation while avoiding free-free absorption in a high-density setting (Kulkarni et al. 2014; Murase et al. 2016), an absence of increased FRB rates toward the Galactic plane (Champion et al. 2016), limits on source repetition (Petroff et al. 2015b), and the absence of known or apparent variable stars in association with most known FRBs (Maoz et al. 2015).

In this paper we present a search for untriggered (sub-threshold) gamma-ray FRB counterparts. This is not the first search for gamma-ray counterparts to FRBs. Following identification of FRB 121102 as a repeating source, Scholz et al. (2016) reviewed Swift BAT above-threshold, Fermi Gamma-ray Burst Monitor (GBM; Meegan et al. 2009) subthreshold, and Fermi Large Area Telescope (LAT; Ackermann et al. 2012) subthreshold datasets without identifying any significant transient gamma-ray activity from that source.

Tendulkar et al. (2016) considered a set of during-, pre-, and post-FRB gamma-ray observations from the Swift BAT, Fermi GBM, and Konus-Wind (Aptekar et al. 1995) instruments, without identifying any likely gamma-ray counterparts, and derived the first limits on any FRB-like counterpart to the 2004 December 27 giant gamma-ray flare from SGR 1806–20.

Taking an alternate approach, Bannister et al. (2012) implemented a program of rapid-response radio observations of gamma-ray bursts (GRBs) using the Parkes Observatory 12 m dish and reported two candidate associated radio bursts (for GRBs 100704A and 101011A) from nine observed GRBs. However, these candidates may be artifacts of radio frequency interference; null results from a more sensitive subsequent search by Palaniswamy et al. (2014), and other GRB rapid-response experiments discussed therein, lend weight to this interpretation.

Going forward, the promise of VLA or other interferometric detections of FRBs is substantial (Law et al. 2015), as these would yield sub-arcsecond positions from the burst data alone. Such positions could yield high-confidence host galaxy identifications without the need to identify non-radio transient counterparts.

Apart from hopes that FRB counterparts or host galaxies will finally reveal the physical nature(s) of these sources, either counterparts or precise distances will be required if FRBs are to fulfill their substantial promise as probes of cosmology (Ioka 2003; Inoue 2004; Akahori et al. 2016) and fundamental physics (Wei et al. 2015; Wu et al. 2016).

Our manuscript proceeds as follows: We detail the search which yielded discovery of the gamma-ray counterpart to FRB 131104 in Sec. 2, along with our analysis of relevant archival and follow-up observations. In Sec. 3 we explore possible interpretations of our findings, considering FRB models and various high-energy transient source populations. We conclude in Sec. 4.

2. OBSERVATIONS AND ANALYSIS

2.1. *Swift Subthreshold Search*

We carried out a search for untriggered (subthreshold) transient gamma-ray counterparts to all FRBs from the FRBCAT catalog¹ (Petroff et al. 2016), including all reported bursts from the repeating FRB 121102. We examined gamma-ray data from the Swift Burst Alert Telescope (BAT; Barthelmy et al. 2005), in near-continuous operation since November 2004, and from the International Gamma-Ray Astrophysics Laboratory’s IBIS imager (Ubertini et al. 2003), in near-continuous

¹ FRBCAT: <http://www.astronomy.swin.edu.au/pulsar/frbcats/>

operation since October 2002.

During this time, two of 13 non-repeating FRBs and two of 17 bursts from FRB 121102 occurred within the BAT field of view; no FRBs occurred within the IBIS field of view. For each FRB with simultaneous BAT coverage, we retrieved the relevant data from the High-Energy Astrophysics Science Archive Research Center (HEASARC²) and searched for sources within 15' of the FRB coordinates. This radius accounts for uncertainty in the positions of both the radio source (typically localized to a single beam with FWHM $\approx 15'$) and the subthreshold BAT source candidates (having 90%-containment radii $r_{90} \approx 7'$) that are observed in these data.

We used the HEASOFT (v. 6.18) software tools and calibration for our high-energy data analyses³. Swift BAT survey data include detector plane histograms (DPHs) of the full-bandpass (15–195 keV) 300 s exposures and scaled detector plane images (DPIs) of the soft-band (15–50 keV) 64 s exposures. We reduced these data using standard procedures, adopting the maximum allowed oversampling parameter of 10, and searched for candidate sources using the *batcelldetect* sliding-cell algorithm. This routine uses local estimates of the background and noise level to identify candidate sources, and then performs a point-spread function (PSF) fit to derive an accurate source position and BAT counts estimate. We estimated uncertainties in source positions (r_{90}) from source significances using the calibration of Baumgartner et al. (2013) (their Eq. 7).

As we are interested in testing the hypothesis of a fixed $S_\gamma : S_{\text{GHz}}$ fluence ratio for FRBs – and as we are interested in non-repeating sources (as candidate catastrophic events) more than in the known repeating source FRB 121102 – we prioritized the search as follows: non-repeating FRBs ordered by decreasing radio fluence, followed by bursts of FRB 121102 ordered by decreasing radio fluence. The results of our search are presented in Table 1.

2.2. Counterpart Discovery

We identified an untriggered gamma-ray transient candidate with signal-to-noise $\mathcal{S} = 4.2\sigma$ in the first search area, that associated with FRB 131104 (Ravi et al. 2015). The transient position is R.A. $06^{\text{h}} 44^{\text{m}} 33^{\text{s}}.12$, Dec. $-51^\circ 11' 31''.2$ (J2000), with $r_{90} = 6'.8$ (Fig. 1). It is located near the edge of the BAT field of view, with only 2.9% of BAT detectors illuminated through the coded mask (2.9% coding), which explains its low significance in spite of a relatively bright inferred

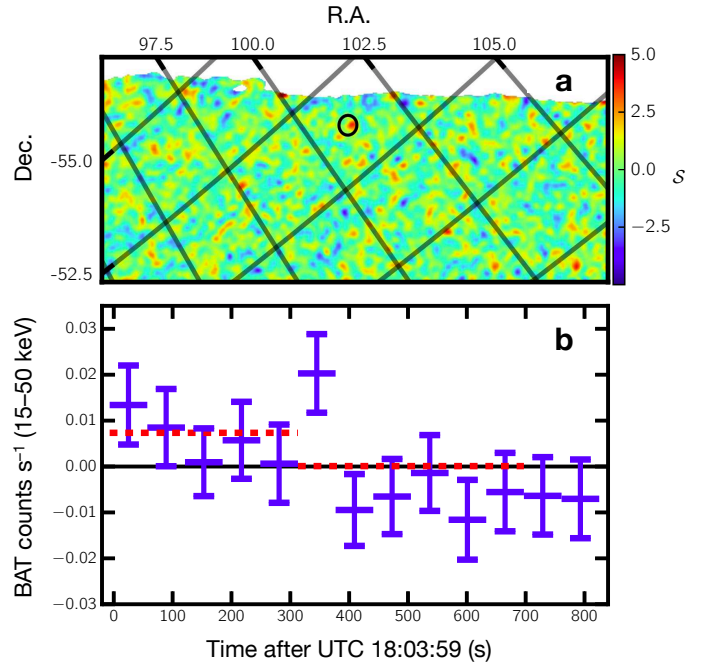


Figure 1. Swift BAT discovery image and light curve for the transient gamma-ray counterpart to FRB 131104, Swift J0644.5–5111. (a) Swift J0644.5–5111 discovery image (15–150 keV; UTC 18:03:52 start; 300 s exposure), showing a small portion of the BAT field of view in tangent plane projection. The search region for FRB 131104 (black circle) is shown; regions with $<1\%$ coding are masked. The point-like excess associated with the gamma-ray transient peaks at signal-to-noise $\mathcal{S} = 4.2\sigma$. (b) Soft-band (15–50 keV) light curve for Swift J0644.5–5111. Time is measured from the FRB detection, UTC 18:03:59. Both 64 s (blue) and 320 s (red dashed) flux measurements are shown; error bars are $\pm 1\sigma$.

fluence. Its sky position is well within the search area, $6'.3$ from the radio receiver pointing, with 50% of its BAT localization probability within the receiver FWHM (Fig. 2). No candidate counterparts are identified for the remaining FRBs with BAT coverage, with results as reported in Table 1.

Since a gamma-ray transient is identified for the highest radio fluence non-repeating FRB in our sample, and since the $S_\gamma : S_{\text{GHz}}$ constraints for the other FRBs are consistent with the ratio inferred for FRB 131104, this is consistent with our hypothesis and first test, and we adopt a trials factor of one for assessing the significance of the counterpart.

We determine this significance by examining 1429 archived BAT survey pointings with exposure times 200 s to 400 s that were taken over the one-year period June 2015 to May 2016. On average each of these survey images has 46.3 transient candidates with $\mathcal{S} \geq 4.2\sigma$ at $>1\%$ coding; although some may be cosmic sources, for present purposes we treat them all as noise fluctuations. The density of candidates per unit solid angle varies across the field of view, so we focus on a rectangular region of the BAT image plane, centered on the transient position in tangent plane coordinates. Within

² HEASARC: <http://heasarc.gsfc.nasa.gov/>

³ HEASOFT: <http://heasarc.nasa.gov/lheasoft/>

Table 1. Swift BAT observations of FRBs

FRB	R.A.	Dec.	S_{GHz} (Jy ms)	UTC	BAT Δt (s)	S_γ (10^{-6} erg cm^{-2})	$\log_{10} \eta$
131104	101.062	-51.278	2.33	2013-11-04 18:03:59	-7, +293	4.0 ± 1.8	5.8 ± 0.2
"	"	"	"	"	+293, +593	<2.8	n/a
110626	315.929	-44.739	0.56	2011-06-26 21:33:15	-84, +216	<1.1	>5.7
121102 (2)	82.992	33.134	0.11	2015-05-17 17:42:09	-46, +254	<2.4	>4.6
121102 (3)	82.992	33.134	0.10	2015-05-17 17:51:41	-18, +248	<2.0	>4.7

Note—FRB radio properties from FRBCAT (Petroff et al. 2016). BAT pointing Δt (start, stop) intervals are given with respect to the quoted topocentric FRB time; gamma-ray fluences S_γ (15–150 keV) are calculated using the best-fit photon index $\Gamma = 1.16$ power-law spectrum for FRB 131104 and assuming a photon index $\Gamma = 2$ power-law spectrum for the other events; radio to gamma-ray fluence ratios $\eta \equiv S_{\text{GHz}}/S_\gamma$ are in units of $\text{Jy ms erg}^{-1} \text{cm}^2$. BAT survey image ObsIDs are: 00571830037 (FRB 131104), 00040453002 (FRB 110626), and 00036376034 (for both bursts of FRB 121102). Further details on FRB radio properties are available from FRBCAT.

this region, which has area 16 deg^2 (0.36% of the field of view), we find an average of 0.106 ± 0.009 transient candidates per survey pointing. This average density of candidates does not vary systematically with pointing coordinates, exposure time, or date, over the set of BAT pointings. The resulting p -value, corresponding to the number of expected candidates in a single $15'$ search radius, is $p = 0.13\%$, corresponding to Gaussian confidence level $\mathcal{C} = 3.2\sigma$.

We also estimate the significance of the association by an alternate Bayesian approach that does not require us to define a search area in advance. Instead, we make a point comparison of the probability density for an FRB-associated transient (at the maximum-likelihood position of the gamma-ray transient) to the probability density for a noise fluctuation. The former will be distributed according to the FRB positional uncertainty (derived below), while the latter will be uniform over the larger rectangular test region. Because the transient is located 1.2σ from the FRB coordinates (distance $d = 6.25'$, $\sigma = 5.2'$), the FRB counterpart probability density is $2.85 \times 10^{-3} \text{ arcmin}^{-2}$; while the background source density is $1.84 \times 10^{-6} \text{ arcmin}^{-2}$. Hence an association is preferred by an odds ratio of 1552:1, corresponding to Gaussian confidence level $\mathcal{C} = 3.4\sigma$.

As both metrics exceed the 3σ threshold common for counterpart identification in astrophysics, we consider the transient confirmed and designate it Swift J0644.5–5111, the first non-radio counterpart to any FRB. Its properties are summarized in Tables 1 and 2.

2.3. Counterpart Properties

We first seek to refine the location for FRB 131104 by combining radio and gamma-ray constraints. This requires a quantitative form for the radio localization; since this has not previously been derived in a rigorous fashion, we describe our approach here.

Table 2. Properties of FRB 131104

Joint	R.A.	$06^{\text{h}} 44^{\text{m}} 27^{\text{s}}.06$
	Dec.	$-51^\circ 12' 54''.0$
	r_{90}	$5'.78$
Radio	UTC	18:03:59
	S_{GHz}	2.33 Jy ms
	DM	$779 \pm 1 \text{ pc cm}^{-3}$
	z_{max}	0.55
γ -ray	T_{90}	$377 \pm 24 \text{ s } (1\sigma)$ >100 s (90%-c.l.)
	PL Γ	$1.16^{+0.68}_{-0.78}$
TB	$S_{\gamma,-6}$	4.0 ± 1.8
	kT	$200^{+\infty}_{-125} \text{ keV}$
	$S_{\gamma,-6}$	3.4 ± 1.5

Note—Radio properties including topocentric burst time (UTC), radio fluence (S_{GHz}), and dispersion measure (DM) are from Ravi et al. (2015), while the maximum redshift for a consensus cosmology (z_{max}) is from Murase et al. (2016). γ -ray and joint properties are from this work. Coordinates for the joint radio + gamma-ray localization are J2000. Spectral parameters for power-law (PL) and thermal bremsstrahlung (TB) fits are quoted with 90%-confidence intervals; gamma-ray fluences $S_{\gamma,-6}$ (15–150 keV) are in units of $10^{-6} \text{ erg cm}^{-2}$.

We assume an azimuthally-symmetric Gaussian form for the response of the Parkes multibeam receiver #5, which has a quoted FWHM of $15'$ (Ravi et al. 2015). In parallel, we assume an $N(S_{\text{GHz}} > S_0) \propto S_0^{-3/2}$ form for the radio fluence distribution of FRBs (Law et al. 2015). Together, these assumptions imply a two-dimensional Gaussian probability distribution for the location of FRB 131104, with $\sigma = 5.2'$ and 90%-containment radius $r_{90} = 11'.2$, centered on the receiver pointing coordinates R.A. $06^{\text{h}} 44^{\text{m}} 10^{\text{s}}.40$, Dec. $-51^\circ 16' 40''$ (J2000). This puts 92% of the BAT localization within the radio-derived r_{90} . Weighting this localization with the $r_{90} = 6'.75$ localization of the gamma-ray transient yields a

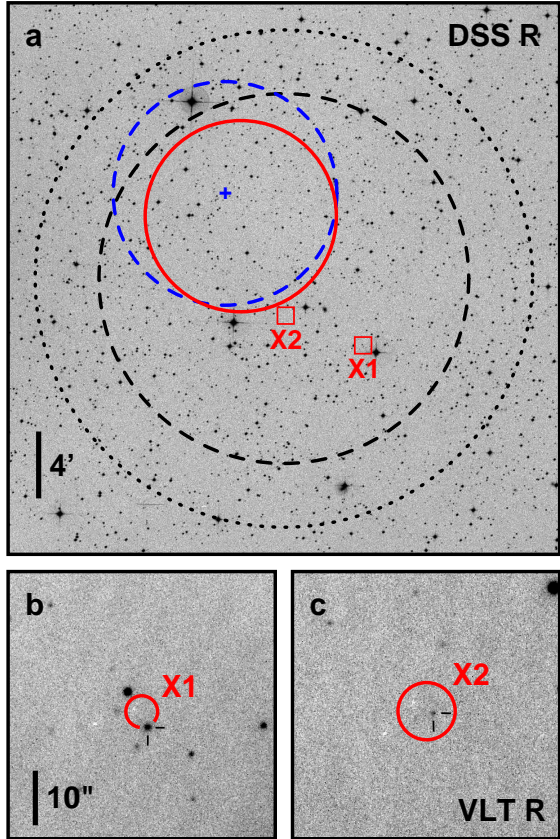


Figure 2. Localizations for FRB 131104 and its transient gamma-ray counterpart, Swift J0644.5–5111. (a) Archival R -band image of the search region ($R = 15'$, black dotted circle) and radio localization ($r_{90} = 11'2$, black dashed circle) for FRB 131104; gamma-ray localization ($r_{90} = 6'8$, blue dashed circle, centered on blue +) for Swift J0644.5–5111; and resulting joint radio + gamma-ray localization ($r_{90} = 5'8$, red solid circle). Positions of the two identified Swift X-ray sources are indicated (red squares). (b) X-shooter R -band image of the Swift J064339.9–512042 region, showing its optical counterpart (ticks), a $z = 0.383$ quasar with $R \approx 19.0$ mag. (c) X-shooter R -band image of the Swift J064409.6–511853 region, showing its optical counterpart (ticks), a $z = 1.525$ quasar with $R \approx 20.8$ mag.

joint localization centered at R.A. $06^{\text{h}}44^{\text{m}}27^{\text{s}}.06$, Dec. $-51^{\circ}12'54''.0$ (J2000), with $r_{90} = 5'78$. This localization is illustrated in Fig. 2 and reported in Table 2.

Examination of archival images of the burst and transient localization region (Fig. 2) does not reveal any prominent Local Group or low-redshift galaxies, nor bright active galaxies, although as noted by Ravi et al. (2015), the field is near the projected tidal limit of the Carina dwarf spheroidal galaxy ($D \approx 100$ kpc) and a projected tidal stream of the Large Magellanic Cloud ($D \approx 50$ kpc). The absence of known or candidate flare stars has been noted by Maoz et al. (2015).

A NASA/IPAC Extragalactic Database (NED⁴) query targeting the predefined search area for FRB 131104

⁴ NED: <https://ned.ipac.caltech.edu>

yields six cataloged galaxies⁵, the quasar QJ0643–5126 ($z = 2.77$), and the IRAS source IRAS F06441–5118. The observed density of resolved galaxies and the presence of a known quasar and an IRAS source are not remarkable for a field of this size at this Galactic latitude. All of these cataloged sources lie well outside the joint localization region except for 2MASX J06435104–5110507, which at $6'$ distance from the center of the joint localization lies just outside its r_{90} .

We generated a spectrum of Swift J0644.5–5111 from the 300s detection image and fitted spectral models within the XSPEC environment. The relatively low signal-to-noise admits a broad range of spectral models, including simple power-law and thermal bremsstrahlung models, which we prefer and present in Tables 1 and 2. Using the best fit power-law we derive a fluence of $S_{\gamma} = 4.0 \pm 1.8 \times 10^{-6}$ erg cm⁻² (15–150 keV).

This implies a radio to gamma-ray fluence ratio of $\log \eta = 5.8 \pm 0.2$ for FRB 131104, where $\eta \equiv S_{\text{GHz}}/S_{\gamma}$ is expressed in units of Jy ms erg⁻¹ cm as defined by Tendulkar et al. (2016). Those authors estimate that the SGR 1806–20 giant flare had $\log \eta < 5.9$ based on modeling of the sidelobe response of the Parkes multibeam receiver (strong constraint), or alternatively, $\log \eta < 7.9$ in an idealized diffraction-limited treatment (weak constraint). Our value for FRB 131104, consistent with the lower limits we derive for FRB 110626 and for two fainter bursts from FRB 121102 (Table 1), is consistent with these upper limits from SGR 1806–20⁶.

For a nominal 10 GHz bandpass and the observed flat or inverted spectrum (Ravi et al. 2015), the integrated radio fluence of FRB 131104 is $S_{\text{radio}} \sim 3 \times 10^{-16}$ erg cm⁻². The gamma-ray counterpart thus increases the energy requirements for this event by a factor of roughly ten billion. (Given its inferred off-center location within the receiver beam, the radio fluence of FRB 131104 may be underestimated.)

We constructed a light curve of Swift J0644.5–5111 using *batcelldetect* to measure the counts from Swift J0644.5–5111 in each of thirteen 64s and two 320s soft-band (15–50 keV) exposures covering the sky po-

⁵ Galaxies within the FRB 131104 radio localization: GALEX-ASC J064303.18–511832.0, 2MASX J06430652–5110339, 2MASX J06434024–5113110, ESO 206-G 022, 2MASX J06435104–5110507, 2MASX J06435472–5118337.

⁶ Tendulkar et al. (2016) derive lower limits on $\log \eta$ for a number of FRBs, including FRB 131104, that are inconsistent with their SGR 1806–20 limit. However, they allow any observation of the FRB position within 10 minutes before or after the burst to limit its gamma-ray fluence, and use a gamma-ray duration of $T_{90} = 0.1$ s to derive limits from non-imaging instruments, the Fermi GBM and Konus-Wind. Their limits are thus not directly comparable with ours, since we analyzed only simultaneous observations by an imaging instrument, the Swift BAT.

Table 3. BAT light curve for Swift J0644.5–5111

t_{start} (s)	Exp. (s)	Flux (cts ks ⁻¹)	Unc.
−7	320	7.34	4.26
−7	64	13.40	8.61
57	64	8.48	8.41
121	64	0.93	7.38
185	64	5.72	8.38
249	64	0.62	8.53
313	320	0.09	3.80
313	64	20.28	8.56
377	64	−9.47	7.82
441	64	−6.54	8.19
505	64	−1.41	8.26
569	64	−11.59	8.69
633	64	−5.57	8.54
697	64	−6.39	8.43
761	64	−7.04	8.57

Note—BAT survey data provide two 320 s integrations and thirteen 64 s integrations over the 15–50 keV bandpass for the pointings covering and immediately subsequent to FRB 131104. Start times t_{start} are measured from the burst time, UTC 2013-11-04 18:03:59. Count rate uncertainties are 1σ .

sition of the transient during and immediately subsequent to the occurrence of FRB 131104. The soft-band light curve, presented in Fig. 1 and Table 3, suggests a transient duration (for 90% of the burst fluence) of $T_{90} \approx 380$ s, extending partway into the next 300 s exposure, which maintained the same pointing.

To quantify the likely burst duration, we adopt a simple “step function” model, assuming a fixed active flux level, a start time $\Delta t = 0$ relative to the FRB, and an end time of $\Delta t = T_{90}$. (We take this approach because the duration of a step-function light curve more closely corresponds to T_{90} than to T_{100} for realistic gamma-ray transient light curves.) We make a χ^2 minimization of this function against the light curve at 64 s resolution, finding a best-fit for $T_{90} = 377$ s ($\chi^2 = 9.9$ for 11 d.o.f.) which extends exactly to the end of the highest-flux sixth time bin, and a 1σ uncertainty range of $T_{90} = 377 \pm 24$ s (Table 2).

We derive a model-independent lower bound on the burst duration by noting that the transient signal-to-noise $\mathcal{S} \propto S_\gamma/\sqrt{T_{90}}$ for relatively plateau-like light curves. Since the transient has $\mathcal{S} = 4.2\sigma$ over 300 s, for $T_{90} \leq 125$ s it would have $\mathcal{S} \geq 6.5\sigma$, leading to a BAT trigger. This is because the BAT flight software continuously evaluates count rates across the detector

in search of excesses (leading to a rate trigger, synthesis of a sky image, and a search for a new point source), and synthesizes sky images at 64 s intervals and multiples thereof during each fixed pointing, in search of new point sources (leading to an image trigger). Due to uncertainty as to the exact shape of the light curve and its timing with respect to BAT integration intervals, we conservatively quote $T_{90} > 100$ s as our 90%-confidence lower limit on the burst duration. Since we cannot exclude the possibility of a very extended duration at a very low flux level, we do not set a 90%-confidence upper bound. If the gamma-ray emission did extend to $t > 293$ s then our quoted fluence will be an underestimate; including the additional fluence seen in the sixth time bin increases the gamma-ray fluence by +66%.

Given its duration ($T_{90} > 100$ s), its spectrum, and the absence of a BAT trigger, non-detections of the source by the Fermi GBM, INTEGRAL SPI-ACS, Konus-Wind, and other Interplanetary Network detectors are not further constraining of the counterpart’s gamma-ray properties.

Given its observed dispersion measure, $DM = 779 \pm 1$ pc cm⁻³, the maximum distance for FRB 131104 is $D \approx 3.2$ Gpc or $z \approx 0.55$ (Murase et al. 2016). This distance estimate will hold approximately in the absence of significant plasma density near the source, and will be reduced if there is any substantial quantity of such local plasma. It is also subject to systematic uncertainties regarding the ionized fraction of gas in the intergalactic medium. At the maximum distance, the implied gamma-ray energy output for FRB 131104 is $E_\gamma \approx 5 \times 10^{51}$ erg.

2.4. Swift Follow-Up

The large inferred gamma-ray energy release for FRB 131104 suggests the possibility of subsequent high-energy afterglow, supernova, or galactic nuclear emissions. We therefore reviewed a set of Swift X-ray and UV/optical observations of the burst position that were taken two days after the original radio discovery, likely in a search for such counterparts (Table 4).

We processed the Swift X-ray Telescope (XRT; Burrows et al. 2005) follow-up data (Swift ObsID 00033033001) with *xrtpipeline*, which provided a clean event list, image, and exposure map for the observations. The XRT data cover 97% of the FRB 131104 radio localization (and 96% of the joint localization) to better than half the nominal 4900 s depth, and were taken in two extended exposures between $t + 2.0$ days and $t + 2.1$ days post-burst. We identified sources using the *wavdetect* routine from the CIAO software package⁷,

⁷ CIAO: <http://cxc.harvard.edu/ciao/>

Table 4. Follow-Up Observations of FRB 131104

Instrument	Band	t_{start} (d)	t_{stop} (d)	Exp. (s)	Cover	Limit	Comments
Swift XRT	0.3–10 keV	2.00	2.10	4912	97%	4×10^{-14}	Excludes brightest 65% of Swift GRB afterglows
Swift UVOT	U	2.00	2.07	157	75%	$32 \mu\text{Jy}$	$U > 19.4$ mag
"	B	2.00	2.07	157	"	59	$B > 19.6$ mag
"	V	2.01	2.08	157	"	132	$V > 18.6$ mag
"	UVM2	2.01	2.10	3432	"	4.3	
"	UVW1	2.00	2.14	322	"	17	
"	UVW2	2.01	2.08	629	"	8.1	
VLT X-shooter	R	2.48	2.55	720	1%	$4.5 \mu\text{Jy}$	Targeting X1 and X2; not used for transient search

Note—Coverage fractions (“Cover”) are quoted for the FRB 131104 radio localization 90%-confidence region (r_{90}), requiring achieved depth of >90% of the exposure time for Swift UVOT and >50% of the exposure time for Swift XRT; coverage fractions for the joint localization 90%-confidence region are 96% (Swift XRT), 92% (Swift UVOT), and 0% (VLT X-shooter), respectively. The Swift XRT X-ray limit is in units of $\text{erg cm}^{-2} \text{s}^{-1}$. UVOT images were searched for new sources by comparison to archival images; absence of deep pre-imaging forestalls a similar search with X-shooter data, which in any case do not provide coverage of the joint localization region.

running against a range of scales, setting the single-trial source threshold at $p = 10^{-6}$, and fixing the PSF FWHM at $12''$.

This analysis yields two high-confidence X-ray sources (Fig. 2) which we designate Swift J064339.9–512042 or X1 (located well outside the joint localization) and Swift J064409.6–511853 or X2 (located $49''$ beyond the joint localization r_{90} , on the edge of the 95%-containment region). For each of these sources, we produced refined positions and r_{90} estimates, optimally-extracted source and background counts, and X-ray spectral fits and flux estimates using the routines of Evans et al. (2009) via the UK Swift Science Data Centre⁸.

These established that Swift J064339.9–512042 or X1 (significance $\mathcal{S} = 5.2\sigma$; 17 counts compared to 1.3 expected from background), is located at R.A. $06^{\text{h}} 43^{\text{m}} 39^{\text{s}}.96$, Dec. $-51^{\circ} 20' 42''.9$ (J2000), with $r_{90} = 3''.1$, and has an estimated X-ray flux of $1.4_{-0.7}^{+1.2} \times 10^{-13} \text{ erg cm}^{-2} \text{ s}^{-1}$ (0.3–10 keV, 90%-confidence bounds); while Swift J064409.6–511853 or X2 ($\mathcal{S} = 3.2\sigma$; 9 counts compared to 0.8 expected from background), is located at R.A. $06^{\text{h}} 44^{\text{m}} 09^{\text{s}}.65$, Dec. $-51^{\circ} 18' 53''.6$ (J2000), with $r_{90} = 5''.6$, and has an estimated X-ray flux of $8.0_{-4.9}^{+13.5} \times 10^{-14} \text{ erg cm}^{-2} \text{ s}^{-1}$. In separate analyses, we confirmed that the arrival times and radial distributions of counts for both sources are consistent with a non-variable point-source nature for each.

Given that X1 is located well outside the joint localization, and that the $z = 1.525$ redshift for X2 (derived below) is beyond the horizon for FRB 131104, we do not consider either source a viable counterpart. We conclude instead that we have established an upper limit of $4 \times 10^{-14} \text{ erg cm}^{-2} \text{ s}^{-1}$ (0.3–10 keV) on the flux of any X-ray counterpart at $t + 2$ days post-burst.

To determine a constraint on GRB afterglow-like counterparts, we considered a library of 192 Swift-detected GRB X-ray afterglows analyzed and modeled by Racusin et al. (2009). Using the power-law decays of these afterglows we interpolated or extrapolated the observed X-ray behavior to $t + 2$ days post-burst, finding that 65% (125 of 192) of these afterglows have inferred fluxes above our limit. Hence we conclude that the XRT observations exclude association of FRB 131104 with the brightest 65% of Swift-type X-ray afterglows.

We processed Swift UV/Optical Telescope (UVOT; Roming et al. 2005) data with *wotskycorr* and *wotimsum*, which yields aspect-corrected coadded images covering 75% of the radio localization (and 92% of the joint localization) to better than 90% of the nominal exposures in each of six UVOT filters: U (157 s exposure), B (157 s), V (157 s), UVM2 (3432 s), UVW1 (322 s), and UVW2 (629 s). We coadd these six images in a search for new or anomalously bright sources by comparison to archival images; none are found within the UVOT area. Using *wotsource*, we derive per-filter flux density upper limits for source-free regions of the image as listed in Table 4; these serve as upper limits for any new point source in the UVOT region.

⁸ Build Swift-XRT Products:
http://www.swift.ac.uk/user_objects/

Review of the Swift GRB Table⁹ shows that there are no examples of Swift burst afterglows detected by UVOT and undetected by XRT; hence we prefer the XRT constraint (excluding the brightest 65% of Swift afterglows) for afterglow-like counterparts.

With respect to supernova (SN) limits, pervasive line-blanketing by metals suppresses SN optical/UV flux at $\lambda < 4000\text{\AA}$, so that the $V > 18.6\text{ mag}$ and $B > 19.6\text{ mag}$ limits (Table 4) are the most useful for SN constraints. Observations at $t + 2$ days post-explosion are sub-optimal for catching associated SNe, as maximum light is achieved after two to three weeks, depending on SN type and explosive energy. Tabulations of SN lightcurves suggest that optical magnitudes at $t + 2$ days are $\Delta M_V \approx 2\text{ mag}$ fainter than peak for type Ibc supernovae (Drout et al. 2011), and likely even further suppressed for type Ia events (Firth et al. 2015), although explosion times for Ia events are not well constrained. As a result, the UVOT limits (ignoring unobserved portions of the joint localization, the 10% probability of the source lying outside the joint localization, and any possible extinction in the host galaxy) are not constraining for the nominal distance $D = 3.2\text{ Gpc}$, as they requires any associated SN to have peak absolute magnitude $M_V > -23.9\text{ mag}$ ($M_B > -22.9\text{ mag}$). UVOT limits become constraining at closer distances; at $D = 320\text{ Mpc}$ the limits of $M_V > -18.9\text{ mag}$ ($M_B > -17.9\text{ mag}$) at peak exclude the brightest $\approx 10\%$ of type Ibc supernovae (Drout et al. 2011) and the brightest $\approx 60\%$ of type Ia supernovae (Ashall et al. 2016).

Unfortunately, the deep southern sky was not being optically surveyed in unbiased fashion for transients and supernovae during the 2013–14 southern summer season. In particular, the Catalina Real-Time Transient Survey (CRTS; Drake et al. 2009) had ceased use of its Siding Springs Observatory 1 m facility in July; the La Silla-QUEST Supernova Survey (LSQ; Walker et al. 2015) was using a drift-scan approach not suited (nor applied) to deep polar regions $\delta \lesssim -40^\circ$; and the Optical Gravitational Lensing Experiment Real-Time Transient Search (OGLE-IV; Wyrzykowski et al. 2014) was focused on transient discovery and variable star studies within and near the Small and Large Magellanic Clouds, without extending as far as the location of FRB 131104. Hence it is not possible to set quantitative limits on the peak magnitude of any associated supernova to FRB 131104 beyond what can be determined from the UVOT observations.

2.5. X-Shooter Follow-Up

We retrieved X-shooter (Vernet et al. 2011) follow-up observations of the two Swift X-ray sources from the ESO Data Archive¹⁰. Each spectroscopic observation was preceded by four 180 s R -band acquisition images. We coadded the undithered exposures for each target, yielding two $1'.5 \times 1'.5$ images with FWHM $\approx 0.7''$ seeing, reaching to roughly $R \approx 22\text{ mag}$ as determined by photometry of unsaturated stars from the USNO-B2.0 catalog (Fig. 2). The image of the region surrounding Swift J064339.9–512042 recovers a likely point-source optical counterpart seen in archival data, which has $R \approx 19.0\text{ mag}$, coordinates R.A. $06^{\text{h}} 43^{\text{m}} 39^{\text{s}}.84$, Dec. $-51^\circ 20' 46''.0$, and $r_{90} \approx 0''.3$. The image of the region surrounding Swift J064409.6–511853 reveals a single candidate point-source optical counterpart with $R \approx 20.8\text{ mag}$, coordinates R.A. $06^{\text{h}} 44^{\text{m}} 09^{\text{s}}.50$, Dec. $-51^\circ 18' 54''.0$, and $r_{90} \approx 0''.3$ (Fig. 2).

Each of the candidate optical counterparts to the two Swift X-ray sources was observed in two dithered 600 s exposures through a $1''$ slit, yielding spectra from each of the three X-shooter spectrographs (UVB, VIS, NIR). We retrieved the Phase 3 data products¹¹, which provide the wavelength-calibrated, rectified, and coadded two-dimensional spectral images and extracted (one-dimensional) spectra for each spectrograph, as processed by the X-shooter Pipeline (Modigliani et al. 2010). We examined the two-dimensional and extracted spectra to determine the nature of each object.

The likely counterpart to Swift J064339.9–512042 (X1) exhibits broad, redshifted emission lines of Mg II (2798Å) and H α with $z \approx 0.38$ and $\Delta v \approx 3500\text{ km s}^{-1}$ (FWHM), demonstrating its nature as a quasar. A weaker, broad H β emission line at this redshift is also present. The redshift is confirmed and refined via narrow emission lines of [O II] (3727Å), [O III] (4959Å), [O III] (5007Å), and [N II] (6584Å), as well as an absorption feature due to the Ca II (3935Å, 3970Å) doublet. These yield a refined redshift of $z = 0.383$, X-ray luminosity $L_X \approx 7.2 \times 10^{43}\text{ erg s}^{-1}$, and absolute magnitude $M_R \approx -22.6\text{ mag}$. This spectroscopic identification confirms the source as the optical counterpart to Swift J064339.9–512042.

The likely counterpart to Swift J064409.6–511853 (X2) exhibits broad, redshifted emission lines of C IV (1549Å), Mg II (2798Å), H β , and H α with $z \approx 1.53$ and $\Delta v \approx 3000\text{ km s}^{-1}$ (FWHM), demonstrating its nature as a quasar. The redshift is confirmed via narrow emission lines of [O II] (3727Å), [O III] (4959Å), and [O III]

¹⁰ ESO Data Archive:
http://archive.eso.org/eso/eso_archive_main.html

¹¹ ESO Phase 3 Archive Interfaces:
http://archive.eso.org/wdb/wdb/adp/phase3_main/form

⁹ Swift GRB Table: http://swift.gsfc.nasa.gov/archive/grb_table/

(5007Å), which yield a refined redshift of $z = 1.525$, X-ray luminosity $L_X \approx 1.2 \times 10^{45} \text{ erg s}^{-1}$, and absolute magnitude $M_R \approx -24.5 \text{ mag}$. This spectroscopic identification confirms the source as the optical counterpart to Swift J064409.6–511853.

2.6. Repeating Counterpart Constraints

Given our findings, and the known existence of repeating FRB sources, we initiated a search for gamma-ray activity in the directions of all known FRBs regardless of relative timing. We established that none of the 1050 triggered Swift GRBs have positions consistent with any of the known FRBs. (We note here the previously published search for Swift and Fermi counterparts to the repeating FRB 121102; [Scholz et al. 2016](#).)

We then examined the complete set of Swift BAT subthreshold events from the Swift archive at HEASARC. We extracted all events that occurred within 2° of any FRB location, excluding FRB 010621, as it lies close to a bright X-ray source. Data run from December 2004 to February 2016, excluding January 2011 (we identified unresolved quality issues with data files for this month), giving a total of 134 months. We searched for an excess of subthreshold events within $15'$ of each FRB position by comparison to the larger region around the FRB (and beyond $15'$; Table 5). Estimated on-axis equivalent exposure times for each FRB position, derived from the exposure map in [Baumgartner et al. \(2013\)](#), are listed. We find no statistically-significant excess for any of the examined positions, and set a 3σ upper limit on the number of such subthreshold events of <14 for the typical such position (corresponding to rates per Ms of on-axis equivalent exposure of $<0.73 \text{ Ms}^{-1}$), and <11 for FRB 121102 ($<0.75 \text{ Ms}^{-1}$). A stacked search over all 15 non-repeater FRB positions gives a limit of <29 excess subthreshold events in all or <2 per FRB position ($<0.11 \text{ Ms}^{-1}$).

3. DISCUSSION

The observation of an energetic gamma-ray counterpart to FRB 131104 challenges FRB models. Nearby Galactic ($D \lesssim 1 \text{ kpc}$) flare stars have been proposed as repeating FRB sources ([Loeb et al. 2014](#)). FRB 131104, however, has no apparent variable stars within its sky localization ([Maoz et al. 2015](#)), and has not been observed to repeat ([Ravi et al. 2015](#)). A local extragalactic origin, as from giant pulses of a pulsar in the Carina dwarf spheroidal galaxy or Magellanic stream ([Ravi et al. 2015](#)), is also excluded, as pulsar giant pulses are not accompanied by gamma-ray emission.

Extragalactic FRBs from hyperflares of young magnetars ([Popov & Postnov 2010](#)), or from rapidly-rotating pulsars or magnetized white dwarfs ([Cordes & Wasserman 2016](#); [Murase et al. 2016](#)), might

Table 5. Swift BAT subthreshold events near FRB positions

FRB	Exp. (Ms)	n_{obs}		n_{exp}	n_{max}	r_{max} (Ms^{-1})
		$(<2^\circ)$	$(<15')$			
121102	14.5	326	4	5.1	10.9	0.75
010125	15.3	672	10	10.5	14.5	0.95
010724	23.9	657	12	10.2	17.6	0.74
090625	23.9	756	12	11.8	16.0	0.67
110220	14.5	450	7	7.0	13.6	0.94
110523	15.3	470	11	7.3	19.1	1.25
110626	14.5	540	4	8.5	7.5	0.52
110703	15.3	501	9	7.8	15.8	1.03
120127	15.3	519	6	8.1	11.0	0.72
121002	21.1	827	10	13.0	12.0	0.57
130626	12.4	515	9	8.0	15.5	1.25
130628	16.3	529	8	8.3	13.8	0.85
130729	14.5	503	3	7.9	6.4	0.44
131104	24.9	818	14	12.8	17.8	0.72
140514	14.5	451	7	7.0	13.6	0.94
150418	17.2	589	6	9.3	9.9	0.57

Note—Equivalent on-axis exposure times in Ms (Exp.) are estimated from Fig. 1 in [Baumgartner et al. \(2013\)](#) and renormalized to the 134 months of our search. n_{obs} is the number of subthreshold events within the specified distance (2° or $15'$) from each FRB, n_{exp} is the expected number of subthreshold events expected within $15'$ based on the number within 2° (excluding those within $15'$), n_{max} is the 3σ upper limit on the number of excess FRB-associated subthreshold events that can be accommodated given the observations, and r_{max} is the 3σ upper limit on the rate of such FRB-associated subthreshold events per Ms on-axis equivalent exposure. FRB 010621 is excluded from this analysis, as it lies close to a bright X-ray source. FRB 121102 is a known repeating FRB source ([Spitler et al. 2016](#)).

be seen repeatedly from sources at $z \lesssim 0.1$, with excess local dispersion produced by a surrounding dense environment such as a wind nebula, supernova ejecta, or the central high-density regions of star-forming galaxies ([Masui et al. 2015](#); [Murase et al. 2016](#); [Piro 2016](#)). In magnetar scenarios this might bring FRB 131104 close enough ($D \lesssim 160 \text{ Mpc}$) to accommodate the maximum expected magnetar flare energy of $E_\gamma \sim 10^{49} \text{ erg}$, which can be achieved if inner magnetic field strengths are $B_c \sim 10^{16} \text{ G}$. However, its gamma-ray emission timescale is $\gtrsim 500\times$ longer than observed for the SGR 1806–20 hyperflare ($T_{90} = 0.2 \text{ s}$; [Hurley et al. 2005](#)).

For all such post-SN or post-merger progenitors, extreme energies $E_\gamma \gtrsim 10^{49} \text{ erg}$ (whether powered by internal magnetic fields or spindown), unless accompanied by beaming, suggest young ages $\tau \lesssim 100 \text{ yr}$. At the same time, the absence of significant free-free absorption along the line of sight requires the surrounding ejecta to be relatively dispersed, $\tau \gtrsim 10$ to 100 yr ([Murase et al. 2016](#)). It is not clear whether these requirements can be met

simultaneously.

Relatively long-duration ($T_{90} \gtrsim 30$ s), smoothly-evolving gamma-ray transients are generic to the relativistic shock breakouts that accompany a variety of massive stellar deaths (Katz et al. 2010; Nakar & Sari 2012), and so might occur at a rate comparable to the $6700 \text{ Gpc}^{-3} \text{ yr}^{-1}$ FRB rate. The thick stellar wind surrounding collapsing massive stars would act as a local source of dispersion (reducing distances, while increasing the inferred volumetric rate); however, the density at the point of shock breakout is large enough that it is not clear how the FRB would not be immediately quenched by free-free and other absorption processes (Kulkarni et al. 2014; Murase et al. 2016). For an energy output $E_\gamma \approx 4 \times 10^{49}$ erg, as seen from the two Swift shock breakout events GRBs 060218 and 100316D (Nakar & Sari 2012), FRB 131104 would be at $D = 290_{-50}^{+90}$ Mpc ($z \approx 0.07 \pm 0.02$). This distance is (roughly) sufficient to keep the X-ray afterglows of these two GRB-SNe below the flux limit of the XRT observations for FRB 131104.

Relativistic tidal disruption events from otherwise quiescent galaxies form another population of long-duration gamma-ray transients seen by Swift (Burrows et al. 2011; Bloom et al. 2011; Zauderer et al. 2011; Cenko et al. 2012; Brown et al. 2015); however, these are rare, with an observed rate of $10^{-3} f_{b,\text{TDE}}^{-1} \text{ Gpc}^{-3} \text{ yr}^{-1}$ (Brown et al. 2015), where the beaming factor is uncertain but typically taken to be $f_{b,\text{TDE}} \geq 10^{-4}$. Moreover, the coherent radio emission mechanism that would generate FRBs in this case is not clear.

FRBs from binary neutron star (BNS) coalescence (Totani 2013), the subsequent collapse of an overmassive neutron star to a black hole (Falcke & Rezzolla 2014; Zhang 2014), or black hole plus neutron star (BH-NS) coalescence (Mingarelli et al. 2015) might yield coincident high-energy emission as a short-hard gamma-ray burst ($T_{90} \lesssim 2$ s; Fox et al. 2005), or subsequently as extended (Kaneko et al. 2015) or flaring (Zhang 2014) emission during the post-burst phase. If the prompt gamma-ray emission were missed due to beaming, yet accompanied by longer-lasting and less-luminous off-axis emission as in “orphan afterglow” scenarios (e.g., Ghirlanda et al. 2015), this would be consistent with the absence of short burst-like emission for FRB 131104; coherent radio emission could be produced immediately pre-merger, although details of the emission mechanism are uncertain. Using the gamma-ray duration constraint and lightcurve data for Swift J0644.5–5111, we constrain the start time of gamma-ray emission to $\Delta t \leq 215$ s after the FRB in this case.

The FRB volumetric rate lower limit of $6700 \text{ Gpc}^{-3} \text{ yr}^{-1}$ is consistent with the upper range of

allowed BNS + BH-NS merger rates (Callister et al. 2016), and with the upper end of beaming-corrected estimates of the short-hard GRB rate (Coward et al. 2012). These merger rates should be quickly refined or reduced via upcoming runs of the advanced gravitational wave facilities (Callister et al. 2016).

Assuming a beaming-corrected short-hard GRB rate of $R_{\text{SHB}} \sim 1000 \text{ Gpc}^{-3} \text{ yr}^{-1}$, then, based on the sensitivity of BAT with the imaging trigger, the beaming factor of any associated extended emission must be $f_{b,\text{SHB-EE}} \lesssim 3 \times 10^{-2}$, which is not much larger than the estimated beaming factor of the prompt emission, $f_{b,\text{SHB}} \sim 10^{-2}$ (Coward et al. 2012). Thus, the BNS scenario for FRBs and short-hard GRBs predicts that coincidences between FRBs and short gamma-ray bursts should be almost as common as the “off-axis”-type coincidence that could be invoked to explain FRB 131104.

The large gamma-ray energy of $E_\gamma \sim 5 \times 10^{51}$ erg is encouraging for detection of counterparts with late-time follow-up observations. If accompanied by a relativistic jet with comparable kinetic energy, it implies that FRB X-ray and radio afterglows can be detected as with short-hard GRBs.

If some FRBs are accompanied by gamma-ray transients with supernova or luminous afterglow counterparts, then these offer the prospect of arcsecond localizations, host galaxy identifications, and distance measurements for FRBs, and hence may facilitate application of FRBs to outstanding questions of fundamental physics (including tests of Lorentz invariance and the equivalence principle) and cosmology (Ioka 2003; Inoue 2004; McQuinn 2014; Wei et al. 2015; Wu et al. 2016; Akahori et al. 2016).

Had it been viewed at close to normal incidence ($>90\%$ coding), Swift J0644.5–5111 would have had $\mathcal{S} \gtrsim 20\sigma$, almost certainly yielding a BAT image trigger. Past Swift image trigger events include the relativistic shock breakout GRB-SNe and relativistic tidal disruption events already mentioned, along with multiple additional long (Starling et al. 2011) and “ultra-long” bursts (Levan et al. 2014), which have been argued to represent a distinct class of GRBs.

This presents a puzzle of interpretation because of the profound mismatch in inferred rates between the known varieties of long-duration gamma-ray transient – we estimate $\sim 25 \text{ yr}^{-1}$ above BAT threshold – and the FRB all-sky rate of 2100 day^{-1} (Champion et al. 2016). While we cannot hope to resolve this mismatch with just one counterpart and one upper limit among two non-repeating FRBs observed (Table 1), we do note the following: (1) The existence of the repeating FRB 121102, combined with limits on repetition from other FRBs including FRB 131104, already suggests that multiple source populations contribute to the FRB phenomenon;

(2) The limits on repeating gamma-ray transients derived here strongly suggest that repeating-type FRBs do not have gamma-ray counterparts; (3) The long timescale of Swift J0644.5–5111 acts efficiently to hide it from satellite observatories other than Swift; and (4) Gamma-ray-bright FRBs may be a minority even among those that generate gamma-ray emissions.

4. CONCLUSIONS

Our discovery that some FRBs are accompanied by energetic gamma-ray transients dramatically alters the basic picture of these events. To date the FRBs have excited interest on the basis of their short timescales, likely-cosmological distances, and high event rates; however, received fluences of the events have been small, implying potentially modest energy requirements ($E_{\text{radio}} \sim 4 \times 10^{41}$ erg in this case). The gamma-ray energy requirement for FRB 131104 is more than 10^9 times greater, with dramatic implications for source models and a substantial improvement in the prospects for long-lived counterparts, including X-ray and radio afterglows. The increased energy scale also raises the consequences of the FRB phenomenon for the bursts' host galaxies and their evolution, as well as (for relatively young progenitors) the evolution of their star-forming regions.

Looking forward, this result should further energize efforts aimed at real-time discovery and multiwavelength follow-up observations of FRBs. We expect these searches will now routinely extend into the subthreshold regime for wide-field experiments such as Swift, Fermi, and the High Altitude Water Cherenkov facility (HAWC; DeYoung & HAWC Collaboration 2012); and to multimessenger facilities including IceCube (Achterberg et al. 2006), ANTARES (Ageron et al. 2011), Pierre Auger (Abraham et al. 2010), and the gravitational wave observatories (Weinstein et al. 2012).

Such a joint and coordinated search for counterparts would be a natural project for the Astrophysical Multimessenger Observatory Network (AMON; Smith et al. 2013) now under construction at Penn State. The most promising immediate prospects probably relate to rapid and sustained X-ray and radio afterglow and nearby ($z \lesssim 0.1$) supernova searches in the wake of each bright and well-localized FRB.

While our finding resolves a pressing question regarding the FRBs – do they exhibit non-radio counterparts – and yields important clues as to the nature of this event, it simultaneously bolsters the case for multiple FRB source populations. These likely wait to be revealed by future radio searches and rapid-response follow-up observations across the electromagnetic spectrum and via multimessenger facilities.

We gratefully acknowledge support from Penn State's Office of the Senior Vice President for Research, the Eberly College of Science, and the Penn State Institute for Gravitation and the Cosmos. K.M. acknowledges support by NSF Grant No. PHY-1620777, while P.M. acknowledges NASA support via grant NNX13AH50G. This research has made use of data and software provided by the High Energy Astrophysics Science Archive Research Center (HEASARC), which is a service of the Astrophysics Science Division at NASA/GSFC and the High Energy Astrophysics Division of the Smithsonian Astrophysical Observatory. It has also made use of data and online tools supplied by the UK Swift Science Data Centre at the University of Leicester, and of data obtained from the ESO Science Archive Facility.

Facilities: Swift (BAT, XRT, UVOT), VLT (X-Shooter)

Software: HEASOFT, IDL, SciPy, CIAO

REFERENCES

- Abraham, J. et al. 2010, Nuclear Instruments and Methods in Physics Research A, 613, 29
- Achterberg, A. et al. 2006, Astroparticle Physics, 26, 155
- Ackermann, M. et al. 2012, ApJS, 203, 4
- Ageron, M. et al. 2011, Nuclear Instruments and Methods in Physics Research A, 656, 11
- Akahi, T., Ryu, D., & Gaensler, B. M. 2016, ArXiv.org, 1602.03235
- Aptekar, R. L. et al. 1995, Space Sci. Rev., 71, 265
- Ashall, C., Mazzali, P., Sasdelli, M., & Prentice, S. J. 2016, MNRAS, 460, 3529
- Bannister, K. W., Murphy, T., Gaensler, B. M., & Reynolds, J. E. 2012, ApJ, 757, 38
- Barthelmy, S. D. et al. 2005, Space Sci. Rev., 120, 143
- Baumgartner, W. H., Tueller, J., Markwardt, C. B., Skinner, G. K., Barthelmy, S., Mushotzky, R. F., Evans, P. A., & Gehrels, N. 2013, ApJS, 207, 19
- Bloom, J. S. et al. 2011, Science, 333, 203
- Brown, G. C., Levan, A. J., Stanway, E. R., Tanvir, N. R., Cenko, S. B., Berger, E., Chornock, R., & Cucchiara, A. 2015, MNRAS, 452, 4297
- Burrows, D. N. et al. 2005, Space Sci. Rev., 120, 165
- 2011, Nature, 476, 421
- Callister, T., Kanner, J., & Weinstein, A. 2016, ApJ, 825, L12
- Cenko, S. B. et al. 2012, ApJ, 753, 77
- Champion, D. J. et al. 2016, MNRAS, 460, L30
- Cordes, J. M. & Wasserman, I. 2016, MNRAS, 457, 232
- Coward, D. M. et al. 2012, MNRAS, 425, 2668
- DeYoung, T. & HAWC Collaboration 2012, Nuclear Instruments and Methods in Physics Research A, 692, 72
- Drake, A. J. et al. 2009, ApJ, 696, 870
- Drout, M. R. et al. 2011, ApJ, 741, 97
- Evans, P. A. et al. 2009, MNRAS, 397, 1177
- Falcke, H. & Rezzolla, L. 2014, A&A, 562, A137
- Firth, R. E. et al. 2015, MNRAS, 446, 3895
- Fox, D. B. et al. 2005, Nature, 437, 845

- Ghirlanda, G. et al. 2015, *A&A*, 578, A71
- Hurley, K. et al. 2005, *Nature*, 434, 1098
- Inoue, S. 2004, *MNRAS*, 348, 999
- Ioka, K. 2003, *ApJ*, 598, L79
- Kaneko, Y., Bostancı, Z. F., Göğüş, E., & Lin, L. 2015, *MNRAS*, 452, 824
- Katz, B., Budnik, R., & Waxman, E. 2010, *ApJ*, 716, 781
- Keane, E. F. et al. 2016, *Nature*, 530, 453
- Kulkarni, S. R., Ofek, E. O., Neill, J. D., Zheng, Z., & Juric, M. 2014, *ApJ*, 797, 70
- Law, C. J. et al. 2015, *ApJ*, 807, 16
- Levan, A. J. et al. 2014, *ApJ*, 781, 13
- Loeb, A., Shvartzvald, Y., & Maoz, D. 2014, *MNRAS*, 439, L46
- Lorimer, D. R., Bailes, M., McLaughlin, M. A., Narkevic, D. J., & Crawford, F. 2007, *Science*, 318, 777
- Maoz, D. et al. 2015, *MNRAS*, 454, 2183
- Masui, K. et al. 2015, *Nature*, 528, 523
- McQuinn, M. 2014, *ApJ*, 780, L33
- Meegan, C. et al. 2009, *ApJ*, 702, 791
- Mingarelli, C. M. F., Levin, J., & Lazio, T. J. W. 2015, *ApJ*, 814, L20
- Modigliani, A. et al. 2010, in *Proc. SPIE, Vol. 7737, Observatory Operations: Strategies, Processes, and Systems III*, 773728
- Murase, K., Kashiyama, K., & Mészáros, P. 2016, *MNRAS*
- Nakar, E. & Sari, R. 2012, *ApJ*, 747, 88
- Palaniswamy, D., Wayth, R. B., Trott, C. M., McCallum, J. N., Tingay, S. J., & Reynolds, C. 2014, *ApJ*, 790, 63
- Petroff, E. et al. 2015a, *MNRAS*, 447, 246
- 2015b, *MNRAS*, 454, 457
- Piro, A. L. 2016, *ApJ*, 824, L32
- Popov, S. B. & Postnov, K. A. 2010, in *Evolution of Cosmic Objects through their Physical Activity*, ed. H. A. Harutyunian, A. M. Mickaelian, & Y. Terzian, 129–132
- Racusin, J. L. et al. 2009, *ApJ*, 698, 43
- Ravi, V., Shannon, R. M., & Jameson, A. 2015, *ApJ*, 799, L5, 1
- Roming, P. W. A. et al. 2005, *Space Sci. Rev.*, 120, 95
- Scholz, P. et al. 2016, *ArXiv.org*, 1603.08880, 1
- Smith, M. W. E. et al. 2013, *Astroparticle Physics*, 45, 56
- Spitler, L. G. et al. 2016, *Nature*, 531, 202
- Starling, R. L. C. et al. 2011, *MNRAS*, 411, 2792
- Taylor, M. et al. 2014, *ApJ*, 792, 135
- Tendulkar, S. P., Kaspi, V. M., & Patel, C. 2016, *ApJ*, 827, 59
- Thornton, D. et al. 2013, *Science*, 341, 53
- Totani, T. 2013, *PASJ*, 65
- Ubertini, P. et al. 2003, *A&A*, 411, L131
- Vernet, J. et al. 2011, *A&A*, 536, A105
- Walker, E. S. et al. 2015, *ApJS*, 219, 13
- Wei, J.-J., Gao, H., Wu, X.-F., & Mészáros, P. 2015, *Physical Review Letters*, 115, 261101, 1
- Weinstein, A. J., Ligo Scientific Collaboration, & Virgo Collaboration 2012, *Journal of Physics Conference Series*, 375, 062001
- Williams, P. K. G. & Berger, E. 2016, *ApJ*, 821, L22, 1
- Wu, X.-F. et al. 2016, *ApJ*, 822, L15
- Wyrzykowski, L. et al. 2014, *AcA*, 64, 197
- Zauderer, B. A. et al. 2011, *Nature*, 476, 425
- Zhang, B. 2014, *ApJ*, 780, L21